ISBN: 978-3-95450-204-2 ISSN: 2673-5350 doi:10.18429/JACoW-IBIC2019-WEBO03

DEVELOPMENT OF MTCA.4-BASED BPM ELECTRONICS FOR SPring-8 UPGRADE

H. Maesaka†, T. Fukui, RIKEN SPring-8 Center, Sayo, Hyogo, 679-5148, Japan
H. Dewa, T. Fujita, M. Masaki, C. Saji, S. Takano[1], JASRI/SPring-8, Sayo, Hyogo, 679-5198, Japan
[1]also at RIKEN SPring-8 Center, Sayo, Hyogo, 679-5148, Japan

Abstract

We have developed a new BPM readout electronics based on the MicroTCA.4 standard for the low emittance upgrade of SPring-8 (SPring-8-II). The main requirements for the BPM system are a highly stable closed-orbit distortion measurement within 5 μm error for 1 month and a high-resolution single-pass BPM better than 100 μm rms for a 0.1 nC injected bunch. We designed an rf front-end rear transition module (RTM), which has band-pass filters, low-noise amplifiers, step attenuators, and pilot tone generators. BPM signals from the RTM are detected by a high-speed digitizer advanced mezzanine card (AMC) developed for the new low-level rf system of SPring-8. The beam position is calculated by the FPGA on the AMC in realtime. We evaluated the performance of the new BPM electronics at the present SPring-8 storage ring with a prototype BPM head for the SPring-8 upgrade. The single-pass resolution was estimated to be better than 30 μm rms for a 0.13 nC single bunch. The long-term stability was confirmed to be within 5 μm peak-to-peak for one or two weeks if the filling pattern was not changed. Thus, the new BPM system satisfies the requirements from SPring-8-II.

INTRODUCTION

To provide much more brilliant X-rays to users, the SPring-8 upgrade project, SPring-8-II [1], was proposed and we are developing accelerator components for the upgrade. Compared with the present SPring-8 ring, the beam energy is reduced from 8 GeV to 6 GeV and the magnet lattice is rearranged from double-bend achromat to 5-bend achromat. As a result, the natural emittance is improved from 2.4 nm rad to ~100 pm rad with radiation damping of insertion devices and the X-ray brilliance around 10 keV photons is increased more than 20 times higher than SPring-8.

The beam position monitor (BPM) system for SPring-8-II is required to be more stable and precise than SPring-8 [2]. The beam orbit stability should be 5 μm peak-to-peak for one month to achieve the required optical axis stability of 1 μrad and the source point stability of a few microns. Furthermore, an injected electron beam must be steered within the narrow dynamic aperture of 10 (H) x 2 (V) mm^2 in the commissioning stage. Therefore, the single-pass BPM resolution is demanded to be 100 μm rms for a 0.1 nC injected beam and the electric center should be accurately aligned to the field center of quadrupole and sextupole magnets within 100 μm rms (±200 μm max.).

To fulfill the requirements above, we have developed a stable and precise button-type BPM system consisting of a BPM head, signal cables, and readout electronics. The design and basic performance of the BPM head and cables were already reported in Refs. [2-4]. In this paper, we describe the design and test results of the readout electronics.

DESIGN OF THE BPM ELECTRONICS

Required Functions for the BPM Electronics

For stable and precise BPM measurements, the amplitude from each button electrode must be detected stably and precisely. Since the button-type BPM generates bipolar impulse signals synchronized to the beam, a BPM signal has a main component around the acceleration rf frequency (f_{rf} = 508.76 MHz for SPring-8-II). The beam position is calculated from Δ/Σ,

$$D_x = \left(\frac{\Delta}{\Sigma}\right)_x = \frac{V_1 - V_2 - V_3 + V_4}{V_1 + V_2 + V_3 + V_4},$$

$$D_y = \left(\frac{\Delta}{\Sigma}\right)_y = \frac{V_1 + V_2 - V_3 - V_4}{V_1 + V_2 + V_3 + V_4},$$

$$\begin{pmatrix} X \\ Y \end{pmatrix} \simeq \begin{pmatrix} k_x D_x \\ k_y D_y \end{pmatrix} \quad (1)$$

where V_n is the amplitude of each electrode (1: top right, 2: top left, 3: bottom left, 4: bottom right) and k_x and k_y are the conversion coefficients. The BPM head for SPring-8-II has a conversion factor of approximately 7 mm [3]. To suppress the BPM drift within 5 μm, the amplitude stability is required to be 0.1% level (= 2 · 5 μm / 7 mm), corresponding to 0.01 dB. To obtain the BPM resolution of 100 μm, a signal-to-noise ratio of more than 35 (= 0.5 · 7 mm / 100 μm) is needed, corresponding to 31 dB. Thus, highly-stable low-noise rf components and analog-to-digital converters (ADC) are necessary. In addition, an in-situ gain correction mechanism, such as a pilot tone method, should be prepared for better stability.

Furthermore, a high-speed closed-orbit distortion (COD) measurement is needed to prevent any damages of accelerator components and X-ray beamline devices from a large orbit deviation. The beam should be aborted within 1 ms in case of an abnormal beam orbit. Therefore, fast COD data with a 10 kHz update rate is required.

† maesaka@spring8.or.jp

ISBN: 978-3-95450-204-2 ISSN: 2673-5350 doi:10.18429/JACoW-IBIC2019-WEBO03

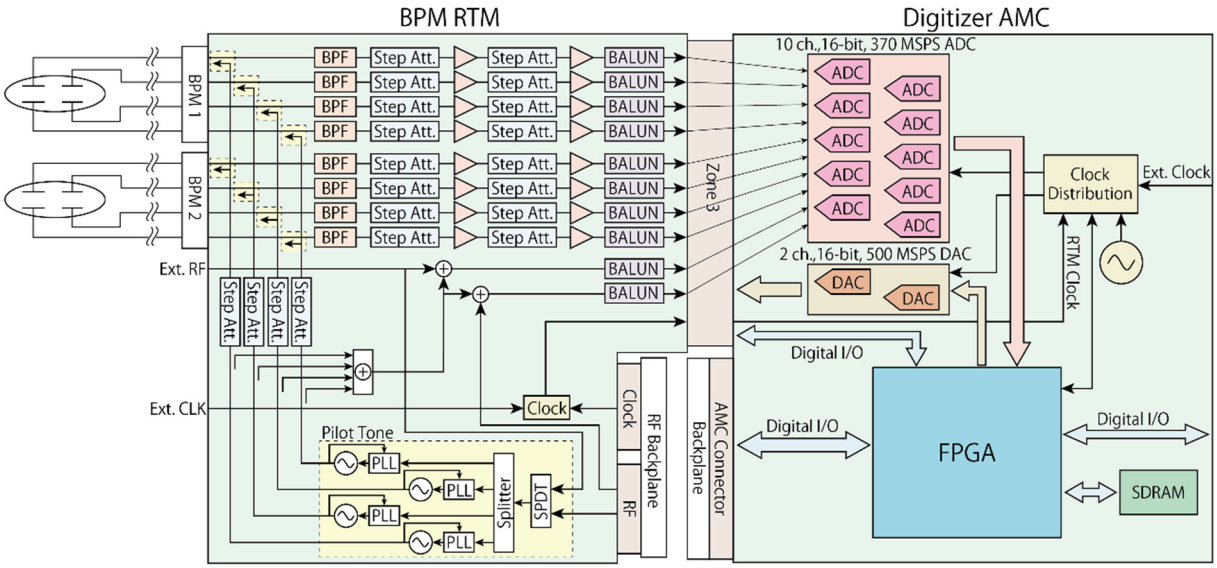

Figure 1: Block diagram of the BPM electronics.

The fast data is also useful for the analysis of fast phenomena.

The number of BPMs in SPring-8-II is reduced to as small as possible and the trouble of a BPM electrode makes a significant impact on the BPM system. Therefore, the BPM system should also be able to calculate the beam position from three electrodes. Since there are four combinations to select three electrodes out of four, we can evaluate the error on the BPM by comparing the four values from three-electrode data [4].

Hardware Design

To fulfill these requirements, we designed the BPM electronics with the following concepts.

- The signal from each electrode is detected by each individual ADC for the high-speed process.
- An under-sampling technique is employed to eliminate the drift of an active analog component.
- Pilot tones are injected to the signal line to monitor the gain drift.
- Variable step attenuators are inserted to the rf front-end for a wide dynamic range.
- A MicroTCA.4 (MTCA.4) platform with an rf backplane [5] is employed since it is already used for the new low-level rf (LLRF) system of SPring-8 [6].

The block diagram of the designed BPM electronics is shown in Fig. 1. We use the same digitizer advanced mezzanine card (AMC) as the LLRF system, which has 10 ch. / 16-bit / 370 MSPS ADCs and a large-scale high-speed FPGA. An rf front-end rear transition module (RTM) was newly designed for the BPM system. Since the digitizer AMC has 10 channels, signals from two BPMs are processed by one board.

On the rf front-end RTM, the f_{rf} component is extracted from an input signal by a SAW band-pass filter with a ~10 MHz bandwidth. The signal level is adjusted to the ADC input by step attenuators and amplifiers. The signal powers from a 0.1 nC single bunch and a 200 mA stored beam are approximately –53 dBm [3] and more than –6 dBm, respectively. The full scale of the ADC is +10 dBm and the noise floor is approximately 60 dB fullscale (dBFS). Since a single-bunch signal amplitude should be around –20 dBFS (–10 dBm) and a COD signal should be around –6 dBFS (+4 dBm), the gain of the amplifier should be more than 40 dB and the maximum attenuation of the step attenuator should be more than 40 dB. Therefore, we use two step-attenuators with 31.5 dB maximum (0.5 dB step), and two amplifiers with 20 dB gain. The signal is finally converted to a balanced differential signal required by the digitizer AMC.

The RTM is also equipped with four pilot tone sources that generate RF signals with frequencies slightly shifted from f_{rf}. These four tones are injected at the input state of the RTM and they are used for the correction of gain drifts etc.

BPM Signal Processing

The BPM signal from the RTM with the frequency of f_{rf} is digitized by an ADC with a 363.40 MHz clock ($= f_{clk} = 5f_{rf}/7$) and an intermediate frequency (IF) data of 145.36 MHz is obtained. The IF data is digitally down-converted to in-phase and quadrature (IQ) baseband signals by a 5-tap digital down converter (DDC) in the FPGA with the following formula,

$$\begin{pmatrix} I_n \\ Q_n \end{pmatrix} = \frac{1}{5}\sum_{k=0}^{5} \begin{pmatrix} \cos\frac{2\pi k}{5} \\ \sin\frac{2\pi k}{5} \end{pmatrix} V_{n-k}.$$

The IQ baseband data is down-sampled to 90.85 MHz ($= f_{clk}/4$), filtered by a finite impulse response (FIR) filter. The IQ data is multiplied by a certain 2 × 2 matrix for the adjustment of the gain and phase of each channel and sent to the COD and SP BPM processes.

ISBN: 978-3-95450-204-2 ISSN: 2673-5350 doi:10.18429/JACoW-IBIC2019-WEBO03

The block diagram of the COD BPM process is illustrated in Fig. 2. The data rate is decimated to f_{rev} for the turn-by-turn (TbT) data, 10 kHz for fast data, and 10 Hz for slow data. Each data stream has a CIC (cascaded integrator comb) filter and an FIR filter to suppress aliasing noise. The bandwidths of these data streams are f_{rev}, 2 kHz, and 2 Hz, respectively.

Since the linear formula in Eq. (1) has a large error around the fringe, the beam position was calculated by a 7th order polynomial of Δ/Σ,

$$\binom{X}{Y} = \sum_{n=0}^{7}\sum_{m=0}^{7-n}\binom{a_{nm}}{b_{nm}} D_x^n D_y^m,$$

where V_n is the amplitude of each electrode, and a_{nm} and b_{nm} are conversion coefficients to the beam position. The error on the position calculation is suppressed to less than 1 μm for the measurement range of $|x|, |y| < 6$ mm with this formula.

The beam position is also calculated from three electrodes in parallel. We calculate four Δ/Σ values,

$$D_1 = \frac{V_1 - V_2}{V_1 + V_2}, \qquad D_2 = \frac{V_3 - V_4}{V_3 + V_4},$$

$$D_3 = \frac{V_1 - V_4}{V_1 + V_4}, \qquad D_4 = \frac{V_3 - V_2}{V_2 + V_3},$$

and the four combinations of the three-electrode beam positions are calculated by,

$$\begin{pmatrix} X_1 & X_2 & X_3 & X_4 \\ Y_1 & Y_2 & Y_3 & Y_4 \end{pmatrix} = \sum_{n=0}^{7}\sum_{m=0}^{7-n}\binom{c_{nm}}{d_{nm}} (D_2^n D_4^m \quad D_2^n D_3^m \quad D_1^n D_3^m \quad D_1^n D_4^m),$$

where c_{nm} and d_{nm} are conversion coefficients to the beam position.

The block diagram of the SP process is shown in Fig. 3. We can apply up to four time-domain masks to the IQ waveform and hence up to four bunches in the ring can be extracted. These signals are sent to the beam position calculation block.

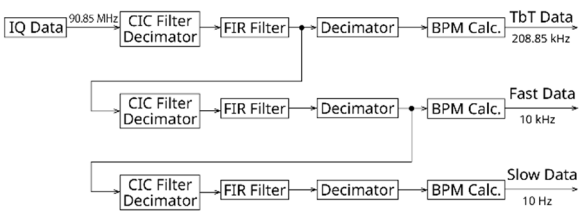

Figure 2: Block diagram of the COD process.

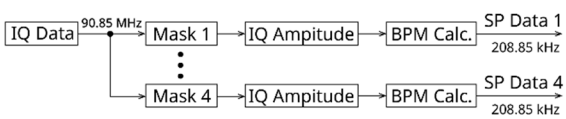

Figure 3: Block diagram of the SP process.

The pilot tone component in the signal is extracted by another DDC with a numerically controlled oscillator (NCO), as shown in Fig. 4. Since the calibration tone is only used for the correction of slow drifts, we change NCO frequency every one second and take four tones one after another.

Figure 4: Block diagram of the pilot tone process.

BEAM TEST RESULTS

We already installed a prototype of the new BPM head to the present SPring-8 ring. Therefore, we evaluated the position resolution and long-term stability with this BPM head. The prototype BPM head has four BPMs (16 electrodes in total) [2]. Two of the BPMs were read out by the new BPM electronics.

Position Resolution

The position resolution was evaluated by comparing the data from the two BPMs. We analyzed both single-bunch SP data and COD data.

Figure 5 (a) shows the scatter plot of the horizontal SP beam positions of a 0.13 nC single bunch when the beam orbit was intentionally vibrated by the pulsed bumper magnet at the injection part. A strong correlation can be seen and the root mean square of the difference between the two BPMs is 31 μm. Assuming the two BPMs have the same resolution, the SP BPM resolution can be estimated to be $31/\sqrt{2} = 22$ μm for a 0.13 nC single bunch, which is well below the required resolution of 100 μm.

Figure 5 (b) shows the horizontal COD fast data of a 30 mA stored beam when the beam orbit was shaken by a fast magnet. This plot also shows a strong correlation and the root mean square of the difference between the two BPMs is 0.55 μm. Therefore, the beam position resolution is estimated to be $0.55/\sqrt{2} = 0.39$ μm. This

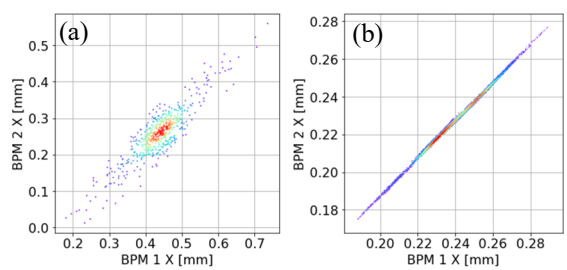

Figure 5: Scatter plots of beam positions from two BPMs. The SP BPM data with a 0.13 nC single bunch is plotted in (a) and the fast COD BPM data with a 30 mA stored current is shown in (b).

ISBN: 978-3-95450-204-2 ISSN: 2673-5350 doi:10.18429/JACoW-IBIC2019-WEBO03

value is 10 – 100 times smaller than the beam size and sufficient for the COD measurement.

Long-Term Stability

We took slow COD data for more than one month during user operation to evaluate long-term stability. The beam current was maintained at 100 mA and the beam orbit was stabilized by the current BPM system. The step attenuator on the RTM was not changed in this period. The BPM electronics was installed in a 19-inch enclosure with a constant temperature and humidity unit. The trend graphs of horizontal COD data from the new BPM system are plotted in Fig. 6. Both two BPM data were stable within ±10 μm and they showed a similar tendency. The temperature and humidity were regulated within 0.04 ℃ and 10%RH peak-to-peak, respectively, in this period.

The stability was also evaluated from the balance error, which was defined to be the maximum difference among the four values from the three-electrode BPM calculation process [4]. The balance error should be independent of the beam position and, therefore, the drift of the BPM system can be evaluated from the balance error. Figure 7 shows the trend graphs of the balance error from the two BPMs (horizontal). Although some small jumps are observed due to the change of the filling pattern (every one or two weeks, indicated by arrows in the figure), the balance error was stable within 10 μm throughout the period. For a constant filling pattern, the drift of the balance error was within 5 μm.

SUMMARY AND OUTLOOK

We designed an MTCA.4-based BPM electronics for SPring-8-II to achieve the required stability of 5 μm in 1 month and the high SP resolution of 100 μm for a 0.1 nC single bunch. We produced a prototype of the rf front-end RTM having band-pass filters, amplifiers, step attenuators, and pilot tone generators. The digitizer AMC is the same as the new LLRF system, but the FPGA firmware of the AMC was substantially modified for the BPM system. The BPM logic in the FPGA provides TbT, fast and slow COD data streams and SP BPM data from up to four bunches. As a result of a beam test, the SP BPM resolution of better than 30 μm was obtained for a 0.13 nC single bunch and the long-term stability of 5 μm peak-to-peak was confirmed for one or two weeks with a constant filling pattern. These results are sufficient for SPring-8-II.

At this moment, the pilot tone is not yet used for the gain calibration. This gain correction function will be implemented in the near future. Some of the BPM electronics in the present SPring-8 ring will be replaced with the new electronics in order to further evaluate the stability and reliability and to utilize fast data for advanced beam diagnostics, such as the fast beam orbit fluctuations, disturbances from fast components, etc.

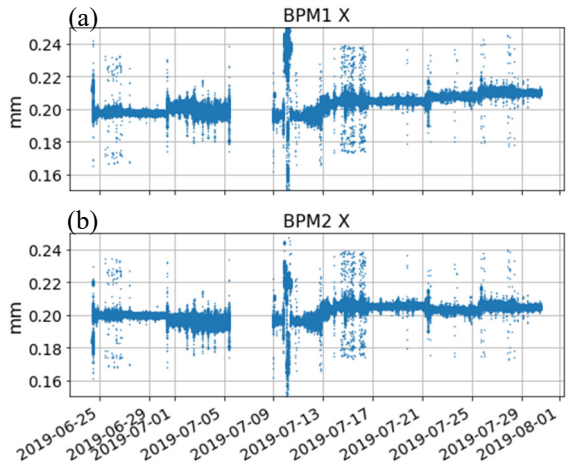

Figure 6: Trend graphs of COD BPM data (horizontal). BPM1 X is plotted in (a) and BPM2 X is in (b).

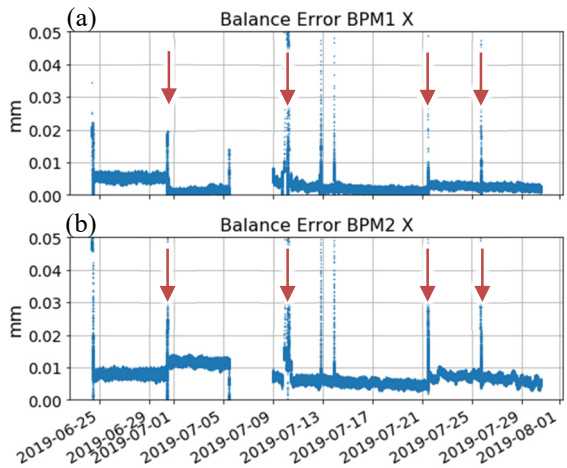

Figure 7: Trend graphs of balance error data (horizontal). BPM1 X is plotted in (a) and BPM2 X is in (b).

REFERENCES

[1] Spring-8-II Conceptual Design Report, Nov. 2014. http://rsc.riken.jp/pdf/SPring-8-II.pdf

[2] H. Maesaka *et al.*, "Development of Beam Position Monitor for the SPring-8 Upgrade", in *Proc. IBIC'18*, Shanghai, China, Sep. 2018, pp. 204–207. doi:10.18429/JACoW-IBIC2018-TUOC04

[3] M. Masaki *et al.*, "Design Optimization of Button-type BPM Electrode for the SPring-8 Upgrade", in *Proc. IBIC'16*, Barcelona, Spain, Sep. 2016, pp. 360–363. doi:10.18429/JACoW-IBIC2016-TUPG18

[4] T. Fujita *et al.*, "Long-term Stability of the Beam Position Monitors at SPring-8", In *Proc. IBIC'15*, Melbourne, Australia, Sep. 2015, pp. 359–363. doi:10.18429/JACoW-IBIC2015-TUPB020

[5] PICMG MicroTCA open standard. https://www.picmg.org/openstandards/microtca/

[6] T. Ohshima, *et al.*, "Development of a New LLRF System Based on MicroTCA.4 for the SPring-8 Storage Ring", In *Proc. IPAC'17*, Copenhagen, Denmark, May 2017, pp. 3996–3999. doi:10.18429/JACoW-IPAC2017-THPAB117